

Turbulence, mass loss and H α emission by stochastic shocks in the hypergiant ρ Cassiopeiae

Cornelis de Jager¹, Alex Lobel^{1,2,*}, and Garik Israelian^{2,3}

¹ SRON Laboratory for Space Research, Sorbonnelaan 2, 3584 CA Utrecht, The Netherlands

² Astronomy Group, Vrije Universiteit Brussel, Pleinlaan 2, B-1050 Brussels, Belgium

³ Instituto de Astrofísica de Canarias, E-38200 La Laguna, Tenerife, Canary Islands, Spain

Received 17 February 1997 / Accepted 28 March 1997

Abstract. The hypergiant ρ Cas is known for its variable rate of mass loss, with an average value of about $10^{-5} M_{\odot} \text{ y}^{-1}$, and the supersonic value for the line-of-sight component of the microturbulent velocity, about 11 km s^{-1} . Emission components in H α suggest the presence of a thermally excited outer atmospheric region.

Since hydrodynamical turbulence in a stellar atmosphere turns rapidly into a field of shock waves, and shock waves are known to be able to initiate a stellar wind and heat stellar atmospheric layers, we have tried to predict the rate of mass loss, the microturbulent velocity component and the observed H α profile by assuming a stochastic field of shock waves. To that end we adopted a Kolmogoroffian spectrum of shock waves, characterized by only one parameter: the maximum Mach number in front of the shocks: $M_{1,\text{max}}$. Behind every shock a thin hot region originates. Spectroscopically, the thermal motions in these sheetlike regions cannot be distinguished from the stochastic hydrodynamic (shock wave) motion component, and therefore these hot regions add to the line broadening and will also contribute to the observed 'microturbulence'.

We find that it is indeed possible to explain the observed rate of mass loss (we derived $\log \dot{M} \approx -5 (M_{\odot} \text{ y}^{-1})$), as well as the high value for the quasi-microturbulence (we calculated $\simeq 12 \text{ km s}^{-1}$). The hot sheets behind the shocks appear to be responsible for the observed 'microturbulence'; this thermal contribution is much larger than that of the hydrodynamic (shock) motions, which is only 0.4 to 0.5 km s^{-1} . Non-LTE calculations of the H α line profile show that the shocks, in association with the observed time-dependent variation of T_{eff} can reproduce aspects of the variable emission in H α .

These three aspects of this star, *viz.* the observed rate of mass loss, the observed supersonic 'microturbulence', as well as the H α line profile can be simulated by one parameter only: *viz.*

$M_{1,\text{max}}=1.06$ to 1.08 , a value that characterizes a fairly weak shock-wave field.

Key words: stars: atmospheres – stars: supergiants – shock waves – turbulence – stars: mass loss

1. The extreme properties of the hypergiant ρ Cas

The star ρ Cas (F8 Ia⁺) is a well-known example of the class of hypergiants. Its luminosity classification (Ia⁺) means that its spectral luminosity characteristics are more extreme than those of class Ia. For ρ Cas the most notorious characteristics are the extreme luminosity, its irregular pulsations, the variable rate of mass loss, and the occurrence of displaced emission components in H α . Beardsley (1961) was the first to notice that emission and he ascribed it to a circumstellar shell. In addition, the central part of the line profile appears to be somewhat filled-in which suggest excited upper chromospheric layers.

The semiregular small-amplitude variability in brightness and radial velocity (Sargent 1961), have a typical brightness fluctuation of 0.2 mag, and an average 'quasi-period' of 300 d. (Zsoldos & Percy 1991). Individual values of the quasi-period range between 280 and 520 d. (Arellano Ferro 1985; Percy et al. 1985; Sheffer & Lambert 1986). Lobel et al. (1994) have studied the observed variations of brightness and radial velocity during 1970 and concluded that these variations cannot be ascribed to strictly radial pulsations.

Next to these small variations there are occasionally sudden larger jumps in brightness, often associated with considerable changes of the spectral type. This latter phenomenon is not yet fully understood, but it is usually ascribed either to larger-than-usual pulsations with a stochastic character, or to excessive mass loss during relatively brief periods. Either phenomenon leads to the formation of an outwardly displaced photosphere (we do not wish to use the term 'pseudophotosphere'), causing an

Send offprint requests to: C. de Jager

* Research Assistant of the Fund for Scientific Research - Flanders (Belgium)

Table 1. Data for ρ Cas

Effective temperature	$T_{\text{eff}} = 7190 \text{ K}$
Effective atmospheric accel.	$g_{\text{eff}} = 2.8 \text{ cm s}^{-2}$
Line-of-sight microturbulent velocity component	$\zeta_{\mu} = 11.1 \text{ km s}^{-1}$
Log of rate of mass loss	$\log \dot{M} = -5 \pm 0.6 \text{ (M}_{\odot} \text{ y}^{-1})$
Log of luminosity	$\log L/L_{\odot} = 5.7$

increase of the stellar surface area and a consequent decrease of the effective temperature.

A matter that may need further investigation is the appearance of blueward displaced emission lines; in July 1960 Sargent (1961) observed Ni I emission lines that were blueward displaced with regard to single absorption lines, with $v_{\text{rad}} \approx 25 \text{ km s}^{-1}$. More recent investigations show as a fairly general rule that the radial velocity measured with the emission lines deviates only little from the system velocity (Sheffer & Lambert 1986). An example is the emission line Na I at 4527 cm^{-1} for which a velocity of -49 km s^{-1} has been found (Lambert et al. 1981). This value, combined with the system velocity (-42 km s^{-1}) yields a residual blueshift of only 7 km s^{-1} . The uncertainty in these velocities is usually given as 1 km s^{-1} , but it may be larger due to blends. Lobel & de Jager (1997) have further studied the blueward displaced ($\leq 10 \text{ km s}^{-1}$) emission components in neutral lines. They do not share the photospheric pulsations, and must be ascribed to a stationary detached shell at some ten to 20 stellar radii from the star.

Published values for the rate of mass loss were summarized by Lobel et al. (1994); they range between -6 and -3 (logarithmic), but the most reliable determinations range between -5.3 and -4.4. The scatter in the data is larger than the mean error of a single unit weight mass loss determination, which is ± 0.37 (de Jager et al. 1988), and therefore seems to be real. A more recent value (Lobel et al. 1997) is -4.5. That value, however, seems to be related to a period of strong outward pulsational motions. In this connection we should note that previously published values for the log of the rate of mass loss, amounting to -2 (Climenhaga et al. 1992) and -2.5 (Gesicki 1992) appeared not to be correct since they are based on a wrong interpretation of seemingly 'double' lines that are actually absorption lines with an emission core (Lobel and de Jager 1997).

The atmospheric properties of the star have been determined recently by Lobel et al. (1994). We give in Table 1 the data, that we will use in this paper. The luminosity is taken from Gesicki (1992).

In this paper we will show that this set of parameters can be reproduced by assuming a photosphere in which a stochastic field of shock waves is running outward. The reasons for assuming a field of shock waves are, first that ρ Cas must have a subphotospheric convection region, wherein turbulence develops, leading to outward running pressure waves. In addition it is known that any field of hydrodynamic waves in a stellar atmosphere transforms rapidly, *i.e.* within the time of one wave period, or after having traveled over a distance of the order of

one wavelength, into a field of shock waves. Hence, beyond a level situated at an average wavelength above the convection layer, the atmospheric motion field must have turned into a field of shock waves.

The general properties of the photospheric wave fields for a number of super- and hypergiants, including ρ Cas, have been derived by de Jager et al. (1991). Since the energies of the hydrodynamic waves are distributed over the wavelengths according to a *spectrum of turbulence* the same must apply to the field of shock waves. We will assume a Kolmogoroff spectrum, since some studies have shown that such a spectrum applies best to stellar photospheres (Dere 1989), and also because the Kolmogoroff spectrum is the only one that is theoretically justified for stellar atmospheric conditions. Once having made that assumption only one parameter is needed for defining all properties of that spectrum. A suitable parameter is the maximum Mach number $M_{1,\text{max}}$ of the spectrum of shock wave energies.

2. Input data for the 'smooth background atmosphere'

Our input data for the 'smooth background atmosphere' are based on an interpolated Kurucz model for the effective temperature and acceleration of the star. A plane model was assumed, since the atmosphere of this star can be treated as being plane, in spite of its extent, because of the star's size relative to the atmospheric thickness (de Jager 1981, p. 195). Onto this 'background atmosphere' we superpose the shock wave field. The numerous shocks are all followed by relatively thin regions of temperature enhancements. Therefore the addition of shocks to the atmospheric model, in the subsequent phase of this investigation, will on the average increase the average photospheric temperature, and integration of that new atmospheric model will yield a higher effective temperature value than the input value.

Therefore it is advisable to start with a lower value for the input effective temperature, and our approach must be an iterative one: after a first input of suitably chosen values for T_{eff} and g_{eff} we derive the interpolated atmospheric (we call it henceforth 'smooth' or 'smooth background') model; then we add the shock wave spectrum, and calculate the stellar flux and effective temperature for this new ('shocked') atmosphere. Iteratively we then search for those input data that yield T_{eff} and g_{eff} values that agree best with the stellar data given in Table 1. After some trials one quickly learns how to choose the input values in order to get rapid agreement with the observed stellar data. There is a slight degree of 'feedback', however: the precise values of the needed input data appear to depend on the assumed shock strengths in the atmosphere, hence on the input value $M_{1,\text{max}}$ of the shock spectrum. This means that the iterative procedure consists essentially of two weakly correlated acts: the choice of T_{eff} and g_{eff} , followed by the choice of $M_{1,\text{max}}$. The first act should lead to an effective temperature and effective acceleration that agree with the observed values, and thereafter the second act should make *two other* observational quantities fitting: the rate of mass loss and the microturbulent velocity component. (We do in this phase not yet consider the H α line profile; this aspect will appear as a bonus from this investigation). Therefore, essentially

our problem reduces to the question whether *one* input value for the shock spectrum can explain *three observables*: mass loss, microturbulence, and the H α line profile.

We next describe the way we calculated the 'smooth background model'. Before doing that we emphasize that it is not necessary to select a model in perfect radiative equilibrium, because the final ('shocked') model anyway will not obey the radiative equilibrium condition. The problem whether a shocked atmosphere is in radiative equilibrium (we think it is not) has not been answered yet and formulating a decisive answer looks a formidable task.

We started with a Kurucz model of which the T_{eff} and g_{eff} values were closest to the expected final input data, and in that model we took the temperature values for five logarithmically equally spaced optical depth values. A spline-type interpolation function was drawn through the data points $\log(T(\tau)) - \log(T_{\text{eff}})$, which yields the function $T(\tau)$ for the adopted T_{eff} and g_{eff} values of this model, and - as we verified - also for the other models that will be met in the course of this investigation. In doing this we based ourselves on the experience that photospheric models have in good approximation the same $(T(\tau) - T_{\text{eff}})$ -relation in any restricted part of the $(T_{\text{eff}}; g_{\text{eff}})$ plane.

The 'smooth background model' is thereupon calculated as follows. For an optical depth $\tau_{\text{Ross}} = 10^{-6}$ we calculate starting values for the pressure P and density ρ by solving for the known $T(\tau = 10^{-6})$ value: $P = g_{\text{eff}} \times 10^{-6} / \kappa_{\text{Ross}}$. The calculation is iterative because κ depends on P and ρ . Integration of $dP/dz = g_{\text{eff}} \times \rho$ and $d\tau/dz = \kappa \times \rho$ (where we write κ for κ_{Ross}) then yields the desired 'smooth background' atmospheric model as a function of the geometrical depth z and the optical depth τ_{Ross} .

For this atmosphere we also need to know the optical and geometrical heights of the top level of the convection zone. This is done by searching for the depth level where $\partial(\log T)/\partial(\log P)_{\text{model}} = \partial(\log T)/\partial(\log P)_{\text{ad}}$. In deriving the last quantity the influence of the ionization of H and He is taken into account.

3. Motion field between shocks

For the following we need relations between the wavelengths of the shocks (*i.e.* the vertical distances between two consecutive shocks), in dependence of the shock velocity amplitudes. To simplify the problem we introduce the following approximation. For any wavelength of the shocks we assume a one-dimensional train of identical, equidistant shocks, moving with constant velocity into the vertical $+z$ -direction, in a homogeneous isothermal medium (Fig. 1). The velocity of propagation is the 'shock velocity' U , which can be derived from the shock relations.

The velocity profile is related to a similar density profile. We write for the log of the density and the shock velocity behind the shocks $\log \rho(z_2)$ and $v(z_2)$. Mathematically, the problem is then to calculate the functions $\log \rho(z)$ and $v(z)$ in a isothermal medium, starting with the above boundary values and for decreasing z , and also to find the point z_1 where $v(z_1) = -v(z_2)$.

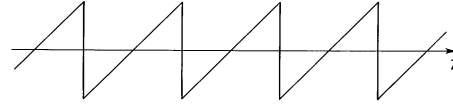


Fig. 1. A train of equal equidistant shocks in a homogeneous and isothermal medium

The wavelength of the shock is then $z_1 - z_2$. We assume an isothermal plasma (admittedly incorrect, but we think acceptable in this phase); hence, we may neglect the energy equation. The equations of conservation of mass and momentum read:

$$d\rho/dt + d(\rho v)/dz = 0. \quad (1)$$

$$d(\rho v)/dt + d(\rho v^2 + P) - \rho g = 0. \quad (2)$$

Introduce $d/dt = d/dz \times dz/dt = -U \times d/dz$. Write further $v' = v/s$, $U' = U/s$, $s^2 = \Gamma_1 \times P/\rho$, where s is the velocity of sound, and introduce $z' = z/H$ with the density scale height $H = RT/\mu g$. Equations (1) and (2) then become dimensionless:

$$d \ln \rho / dz' = [\Gamma_1 (v' - U')^2 - 1 / \Gamma_1]^{-1}, \quad (3)$$

and

$$dv' / dz' = (d \ln \rho / dz') / (U' - v'). \quad (4)$$

We performed a number of numerical integrations and these yielded interpolation relations between the (dimensionless) wavelength L/H , the velocity behind the shock v'_2 , and the shock velocity U' , all three quantities in dependence of the parameters M and Γ . To give an example: for the wavelength L/H a suitable representation reads:

$$L/H = A_p(\Gamma) \times (M - 1) + B_p(\Gamma) \times (M - 1)^2, \quad (5)$$

with

$$A_p(\Gamma) = aa_p + ba_p \times (\Gamma - 1.5) + ca_p \times (\Gamma - 1.5)^2 \quad (6)$$

$$B_p(\Gamma) = ab_p + bb_p \times (\Gamma - 1.5) + cb_p \times (\Gamma - 1.5)^2. \quad (7)$$

We refrain from listing the values of the numerical quantities aa_p through cb_p . We have derived similar equations for the relation between the relative velocity behind the shock v'_2 and the parameters M and Γ . A third set of interpolation equations applies to the dimensionless shock velocity U' . We note that the quantity M is similar to, and will later be used for, the maximum Mach number M_1 , but in the present context it is just a formal parameter introduced in order to link the wavelength L/H , the velocity v'_2 and the shock velocity U' with the values of Γ and M . By means of these equations we can also find the relationship between the wavelength L/H and the dimensionless velocity v'_2 just behind the shock.

4. Stochastic spectrum of shock waves

We next calculate the velocity distribution in the atmosphere defined by a Kolmogoroff spectrum of shock wave energies, in which $M_{1,\max}$ is the maximum Mach number in front of the shocks. The wavelength corresponding to this Mach number is called L_0 . For such a spectrum the relationship between v'_2 or v_2 and L is given by

$$v_2(L)/v_2(L_0) = v'_2(L)/v'_2(L_0) = (L/L_0)^{2/3}. \quad (8)$$

The velocity variation between two equal shocks with a wavelength L is a linear saw-tooth profile, with velocity v_2 behind the leading shock and v_1 in front of the trailing shock (as shown in Fig. 1). If we call this profile $\Upsilon_L(z)$, then the motion field (still without the contribution of the stellar wind) of a Kolmogoroff spectrum of shock waves is

$$v_s(z) = \int_{L_1}^{L_0} (L/L_0)^{1/3} \cdot \Upsilon_L(z + \phi) dL, \quad (9)$$

where ϕ is a phase with a value between 0 and L , which is generated by a random procedure. The introduction of this randomly distributed phase is necessary for simulating the real situation in a stellar atmosphere. In any spectrum of turbulence the phases of the various wave components are distributed randomly. In actual practice, the integration is replaced by a summation. The final velocity profile in the stellar atmosphere is then given by

$$v(z) = v_s(z) + v_w(z), \quad (10)$$

where the value of the wind term v_w is

$$v_w = \dot{M}/4\pi r^2(z)\rho(z). \quad (11)$$

Here, \dot{M} is the rate of mass loss; $r(z)$ is the distance of the point z from the stellar centre. We define the stellar radius by $\tau_{\text{Ross}}=2/3$.

When the velocity profile is known, one has to derive the density- and temperature profiles in the shocked atmosphere. We discuss these matters here for the density and in the next section for the temperature.

The point we make first is that shocks can accumulate. In the actual numerical procedure the velocity $v_s(z)$ or $v(z)$, according to Eqs. (9) and (10) is given for a number of discrete z' points; we used 250 points per average scale height interval. Because of the integration (9) there appear a large number of shocks in the $v(z)$ curve. In order not to overload the program we deleted shocks with a velocity amplitude $< 0.02s$ (s being the local speed of sound), which corresponds to the introduction of an artificial lower limit for L_1 ; we ascertained that the exclusion of these small shocks does not significantly change the overall results. In some cases it may happen, because of the discrete character of the z' axis, that two or more shocks add at a specific z' point, and thus one may even meet the situation (rarely, however) that one obtains shocks that are stronger than the largest input shock. The next step consists therefore of 'sorting' the shocks according to their z -values, taking into account their possible accumulation,

which leads to new $v_2(z)$ values. We will call these sorted shocks the *new shocks*.

At this point shock physics enters into the picture. For each of the *new shocks* thus obtained we know the velocity amplitude and from these values we derive the Mach numbers M_1 in front of the shocks with (cf. Gail et al., 1990, Eq. (56))

$$v_2 = ((\Theta - 1)/2\Theta) \times M_1 \times s, \quad (12)$$

where Θ is the density ratio ρ_2/ρ_1 . For deriving Θ we have to consider that ionization can be important at the temperatures and pressures involved. Therefore we use the generalized version of the Rankine-Hugoniot relations (we abbreviate them as the 'NDJCLA-equations', Eq. (26) of Nieuwenhuijzen et al. 1993). These equations can only be solved iteratively. For the first step of iteration we used the classical Rankine-Hugoniot expressions

$$\Theta = \rho_2/\rho_1 = ((\gamma + 1)M_1^2)/((\gamma - 1)M_1^2 + 2), \quad (13)$$

where $\gamma = c_p/c_v$, calculated for the temperature and pressure at the relevant level, taking ionization into account (for an ideal gas $\gamma = 5/3$), and

$$\Phi = p_2/p_1 = (2\gamma M_1^2 - \gamma + 1)/(\gamma + 1). \quad (14)$$

In order to proceed with the second approximation, we use these quantities for deriving values of γ_H (cf. Nieuwenhuijzen et al. 1993 for the definition of γ_H) and Γ_1 in front and behind the shocks; these quantities are needed for the NDJCLA-relations. Only then can the iteration proceed with the generalized NDJCLA-relations. The iterative derivation of M_1 from v_2 as outlined here is straightforward and it appears to converge well. Fig. 3 (in Sect. 5) is a diagram, calculated for an exaggerated case, $M_{1,\max}=1.5$ in a giant-type atmosphere with $\log g_{\text{eff}}=3$ (hence, not a supergiant), and shows among other things the distribution of the mass density $\log \rho$ in a shocked model atmosphere of this giant star, plotted against the geometrical depth scale. The depth unit is an 'average scale height'. We note that the value $M_{1,\max}=1.5$ is for ρ Cas far too large, and also $\log g_{\text{eff}}$ and the resulting rate of mass loss are by three orders too large but this case demonstrates, better than smaller values, what we want to show.

Once M_1 , v_2 and the other parameters for the *new shocks* are known, it is also possible to find the shock velocity $U = v_1 + s \times M_1$, a quantity that is important for calculating the depth variation of the temperature (next section). It should also be known for evaluating the importance of 'shock cannibalism', the process according to which larger and hence faster moving shocks overtake smaller, hence slower ones, and thus become still larger and faster moving, etc., so that at the very, but indeed: very, long run only large shocks tend to remain. To give an example: for an atmosphere where the waves emerge from a subphotospheric convection region at $\tau \approx 0.3$ (the top of the convection zone in a particular case) the fraction ~ 0.9 of the shocks remains when the shocks have moved from that level until $\tau \approx 0.1$.

5. Temperature distribution in a shocked atmosphere

When the shock parameters such as the density- and pressure-jumps behind the many shocks are known, the temperature is so too, because of the equation of state. In the wake of every shock the temperature excess with respect to the smooth temperature distribution will decline radiatively. For the cooling time we assume (Spiegel 1957)

$$\tau_c = \rho c_v / 16 \kappa \sigma T^3, \quad (15)$$

where κ is the inverse of the photon free path, σ is Stefan-Boltzmann's constant and c_v the specific heat per unit mass at constant volume, calculated including the effects of ionization. For κ we take the Rosseland absorption coefficient. The transformation of the cooling time into a cooling distance goes *via* the shock velocity U . This means that for an observer at a fixed point the temperature will rise at the shock to a value $T_{\text{background}} + \Delta T$, where ΔT is defined by the shock conditions, while it will decrease exponentially with time to the value $T_{\text{background}}$, with the e -folding time defined by Eq. (15). Any instantaneous $T(z)$ -picture of the whole atmosphere will show a number of shock-enhanced temperature jumps ΔT at the respective shocks (each ΔT -value being different, depending on the local shock conditions; *cf.* Fig. 2), followed to lower depths by an exponential decline to $T_{\text{background}}$ (while we know that $T_{\text{background}}$ increases with depth). The value of the exponential is in that case U/τ_c , where U is the shock velocity of the preceding shock.

This picture becomes more complicated at low temperatures, because the cooling time, which is short at high temperatures, increases for decreasing T -values. This poses a computational problem: suppose that an unshocked atmosphere has a low temperature, say 4000 K. Then $\tau_c \gg L/U$, where L is the distance between two successive shocks, and U the shock velocity. That means that in this case a next shock will occur in a medium which still has a higher background temperature than $T_{\text{background}}$, and consequently the shock conditions will not be determined by $T_{\text{background}}$, but by the enhanced temperature in the wake of the preceding shock. The effects of several wakes may thus accumulate as outlined in the cartoon in the lower part of Fig. 2. But this accumulation may go, as it appears, to such an extent that the temperature in the initially low temperature part of the atmosphere would rise to such high values that $\tau_0 \ll L/U$. In that case, however, the above mentioned superposition of temperature wakes would not occur; we would again meet the situation of the upper part of Fig. 2, and the atmosphere would remain overall relatively cool, with only hot sheets after every shock. Sophisticated solutions should be considered for this non-linear feedback problem, but for the time being we are contented with a fairly simple approach. The most direct solution appears to be to start calculations far outside the atmosphere, to eliminate boundary effects. To that end we choose $\tau_{\text{start}} = 10^{-6}$. From there on we number the shocks consecutively, going inward. At a point at a distance d_n behind shock no. n , situated at the geometrical depth z_n , we want to know the total temperature excess due to all shocks preceding that one. We call $T_s(z_n)$ the smooth background temperature at the position

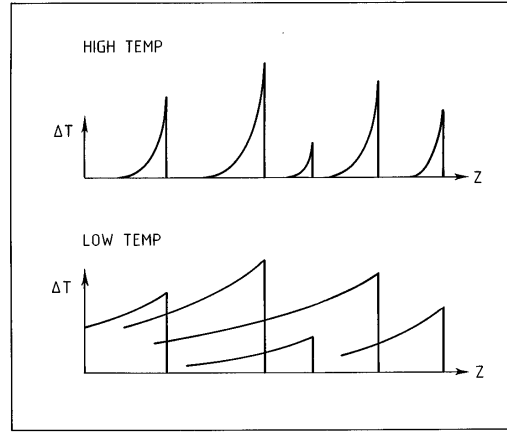


Fig. 2. Accumulation of post-shock high temperature regions. *upper*: high temperature; *lower*: low temperature

z_n . The temperature excess just behind the shock is $T_E(n)$, and the radiative cooling time of that shock is τ_n . At a point at a distance d_1 behind shock no. 1 the temperature of the shocked atmosphere, due to the influence of shock no. 1 is (Fig. 2):

$$T(z_1 - d_1) = T_s(z_1) + T_E(1) \exp(-d_1/U_1\tau_1). \quad (16)$$

Here, $T_s(z_1)$ is still the original 'smooth background temperature', hence the interpolated Kurucz value. For the part of the atmosphere behind the second and subsequent shocks, however, the 'background temperature' at the position of the shocks is no longer the 'smooth background' value but the accumulated effect of the temperature tails of preceding shocks as illustrated in Fig. 2, lower part. If $D_{2,1}$ is the distance between shocks nos. 2 and 1, then the background temperature $T_b(z_2)$ at the position of shock no. 2 is derived from Eq. (16) by writing z_2 for $z_1 - d_1$ and $D_{2,1}$ for d_1 . In general, the 'background' temperature at the position of shock no. n is

$$T(z_n) = T_s(z_n) + \sum_{m=1}^{n-1} T_E(m) \exp(-D_{n,m}/U_m\tau_m), \quad (17)$$

where $D_{n,m}$ is the distance between shocks n and m . Here, any value of $T_E(m)$ is determined by the local thermodynamic conditions at the location of shock no. m ; the temperature at that position is influenced by more than just one preceding shock.

The temperature just after shock no. n is found with the above equation by summing up to $m = n$ instead of to $n - 1$, realizing that $D_{m,m} = 0$. The temperature between shocks n and $n + 1$ at a point z , at distances d_n to shocks no. n is

$$T(z) = T_s(z) + \sum_{m=1}^n T_E(m) \exp(-d_m/U_m\tau_m), \quad (18)$$

for all positive d_m values. In calculating τ_n for the n th shock with Eq. (15) the temperature in that point is derived from Eq. (17). In calculating the values of $T_E(n)$ we used the modified Rankine-Hugoniot relations (Nieuwenhuijzen et al. 1993).

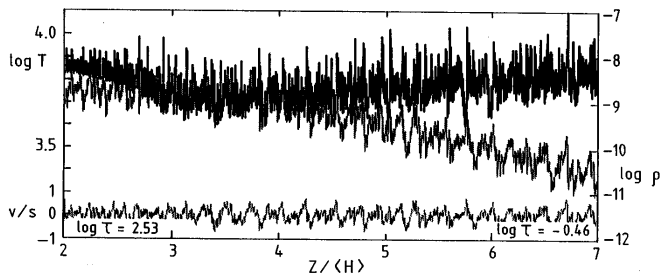


Fig. 3. Variation of $\log T$ (upper), $\log \rho$ (middle) and v/s (bottom) in a shocked atmosphere, plotted on a geometrical depth scale ($z/\langle H \rangle$, where $\langle H \rangle$ is an average scale height). The model is not for ρ Cas, but for a giant model with excessive shocks, viz. $T_{\text{eff}}=7319$ K and $g_{\text{eff}}=10^3$ cm s $^{-2}$, and for $M_{1,\text{max}}=1.5$. These gravity and maximum Mach values are both far too high for the case of ρ Cas, but are introduced to clearly show the features. The figure shows the run of the three variables through a 'window', bordered by $z/\langle H \rangle=2$ and 7; actual calculations were made for $z/\langle H \rangle=0$ to 8. The $\log \tau_R$ -values corresponding to the two border-values of $z/\langle H \rangle$ are printed in the lower corners.

As may be understood, the summed-up temperature is too low for the lowest n -values because of the neglect of the influence of shocks for $\tau \leq 10^{-6}$ but deeper in the atmosphere, for larger n , this is no longer the case. Therefore, our procedure yields unreliable results for very small optical depths, close to $\tau = 10^{-6}$, but it appears to stabilize after a few units of $\log \tau$. In the atmospheric region of interest to us, above $\tau \sim 10^{-3}$, which is 3 τ -decades deeper, such a stable situation appears.

Fig. 3 gives the variation of density, velocity and temperature along the geometrical (z/H_{aver}) scale, thus calculated, in the exaggerated example of the shocked atmosphere presented in Fig. 2.

For the model atmosphere thus obtained, values of the atmospheric parameters should be derived. Hence we calculated:

1. The effective temperature T_{eff} . The computations were simplified by assuming 'gray' absorption coefficients: $\kappa(\lambda) = \kappa_{\text{Ross}}$, but the error thus introduced was reduced to a second order one by working strictly differentially (e.g. in our range of photospheric parameters the difference between the T_{eff} values between the real and gray atmospheres equals 415 ± 10 K).

2. The effective acceleration g_{eff} . This quantity was derived with $g_{\text{eff}} = (\mathcal{R}T/\mu) \times (dz/d \ln \rho)$. It is clear that g_{eff} varies over the depth of the atmosphere. For the time being we do not wish to include that aspect, but we determine one value that may be considered representative for the line-forming part of the atmosphere. Therefore we determined g_{eff} by taking the average over the atmospheric region between τ_{Ross} -values of 1 and 0.001.

6. Shocked atmospheric model on a τ -scale

There is an interesting difference between the shocked atmosphere plotted on a geometrical scale (z -variable) and the one plotted on an optical depth scale (τ -variable), because in the temperature range corresponding to the atmospheres of fairly cool stars the absorption coefficient κ_R increases strongly

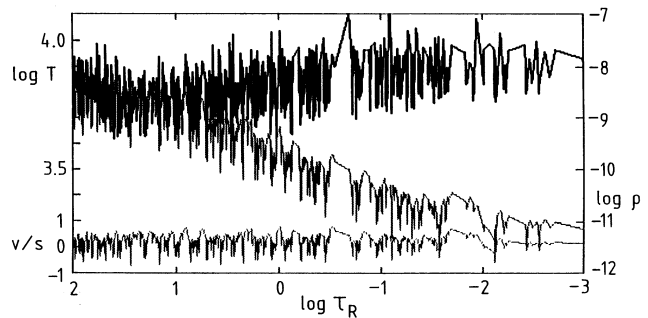


Fig. 4. The shocked atmosphere for the model parameters from Fig. 3, plotted here on a $\log(\tau_R)$ -scale. The curves and ordinates are as in Fig. 3

with T . The consequence is that the geometrically thin high-temperature sheets behind the shocks are fairly thick on a τ -scale. We show this in Fig. 4, which corresponds to the same model as the one shown in Fig. 3.

This effect is important since one observes an atmosphere on a τ scale rather than on a geometrical scale. This makes the high-temperature effects of the atmosphere more pronounced compared to the model plotted on a geometrical scale. Another aspect is that the accumulation of shocks causes a region of enhanced temperature in the upper layers of the atmosphere. This effect mimics a chromosphere.

In our calculations we have artificially included the *dissipation of shock energy*, which is done by keeping the shock amplitude constant with depth. Without dissipation the amplitude would increase with height (because of the decreasing density) but observations of the depth dependence of microturbulence always show this to be practically constant with height (cf. Achmad et al. 1991; Lobel et al. 1992, and references therein to earlier work). This is ascribed to the effect of dissipation. We neglected the heating by shock dissipation, a process usually held responsible for the formation of chromospheres in cool non-magnetic stars. But even with our approach the shocks already produce effects that simulate a chromosphere, as will be shown in Sect. 10. The additional effect of shock dissipation would enhance this phenomenon.

Another consequence refers to the average velocity, observed in the stellar spectrum. While the average velocity of the star is about zero when integrated over the z -scale, this is not the case for the velocity plotted on a τ -scale. For that situation (Fig. 4) one would *observe* a net outstreaming velocity, even for the extreme and hypothetical case when the geometrically averaged velocity would be zero. In such a star, that is not losing mass, one would still *observe an outstreaming velocity*, which is of the order of $s/3$ in the case presented in Figs. 3 and 4.

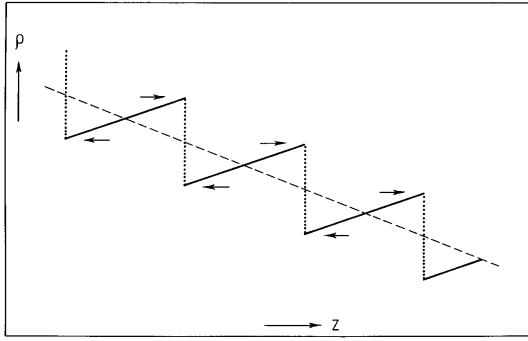


Fig. 5. Shocks initiate mass loss

7. Rate of mass loss

A system of sufficiently strong shock waves in an atmosphere in which the overall density decreases outwardly will lead to a net outflow of matter. This can be shown by integrating

$$\int_{z_{\text{start}}}^{\infty} \rho v dz \quad (19)$$

over a system of equidistant equal shocks superimposed over an outward decreasing density profile (Fig. 5). As is clear from this sketch there is a net outflow of matter.

This is evidently also the case in an atmosphere with a stochastic distribution of shocks. Therefore shocks can initiate mass loss.

In calculating the rate of mass loss the question arises from what level in the atmosphere we should start the outward integration of the integral (19). We decided to place the lower limit z_{start} one scale height above the top of the convection zone. This decision is based on the idea that the convection zone is the region where hydrodynamic turbulence is *generated* and that only above the convection zone, where waves run outward, these will develop into shocks after having gone over a certain distance. For the latter quantity we took one scale height.

Applied to the case of ρ Cas, we derived a rate of mass loss in the range of the observed values $10^{-4.5}$ and $10^{-5.2} M_{\odot} \text{y}^{-1}$. For the actual data reference is made to Sect. 9. We consider this as evidence that a field of shock waves of moderate strength can initiate stellar mass loss, at least in this type of hypergiant. We add that we only claim that shocks *initiate* the process of mass loss, and not that they govern the velocity profile of the stellar winds in remote regions above the photosphere because the shocks will be dissipated over a relatively short distance from the photosphere, while various other effects such as radiation pressure may influence the velocity profile of the wind in the outer parts of the winds.

8. Quasi-turbulence: the notion of microturbulence in a shocked atmosphere

Fig. 4 shows a shocked atmosphere on a $\log \tau$ -scale. Not only the radial velocity varies in a semi-stochastic way, but there are

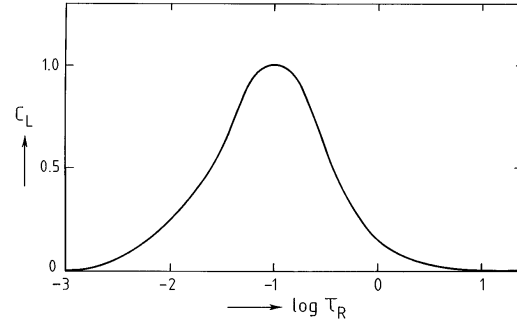


Fig. 6. The assumed contribution function $C_L(\tau_R)$

also strong fluctuations in the temperature, even over relatively short distances. This observation brings us to the subject of the interpretation of the observed values of the 'microturbulent velocity component' ζ_{μ} .

Methods for the diagnosis of stellar atmospheres and the determination of the value of ζ_{μ} are all based on the implicit assumption of an atmosphere with a smooth T -variation. For such an atmosphere equivalent widths of a number of lines of various strengths are calculated, and ensuing systematic differences between calculated and observed equivalent widths of lines are then used to generate new values for quantities such as *e.g.* ζ_{μ} . The point we make here is that *quasi-stochastic temperature variations such as those shown in Figs. 3 and 4, will influence line profiles and their equivalent widths in a way similar to the stochastic hydrodynamic motions, and that it will be hard to distinguish observationally with conventional diagnostic techniques between these two components.*

Therefore we derived a method for predicting the expected value of the microturbulent velocity component ζ_{μ} for shocked atmospheres, on the basis of these two causes for microturbulent line broadening: hydrodynamic motions and temperature fluctuations. We assume as known the variation of variables such as $T(\tau)$, $P(\tau)$, $v(\tau)$, etc. in a shocked atmosphere. In deriving expressions for the calculation of the expected value of ζ_{μ} we further have to take two facts into consideration:

1. Not the whole range of optical depths of the atmosphere contributes to the formation of a line. There is a *contribution function* C_L (Achmad et al. 1991), which varies from one line to the other, but an average function can be given. We have derived such an average contribution function from Achmad et al. (1991) and show it in Fig. 6. As shown in that paper the contribution functions of different lines can vary, but plotted on a $\log \tau$ scale the functions are more or less equal, apart from a possible horizontal shift along the τ -axis; the most extreme case being a downward shift over about one unit in the $\log \tau$ scale. For the time being we use the diagram of Fig. 6, which represents the average line-forming region.

2. Velocity- or temperature variations on very large geometrical length scales do not contribute to microturbulent broadening. There is a *microturbulent filter function* $F_{\mu}(L)$ or $F_{\mu}(k)$, where L is the wavelength of the motion field and $k = L/2\pi$ is the corresponding wave number. This filter function gives the

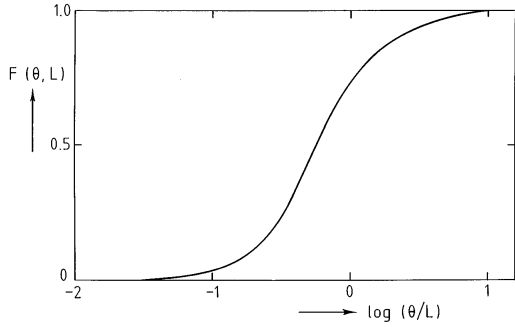


Fig. 7. The filter function $F_\mu(\theta/L)$ for microturbulence

fraction of the kinetic energy of the motion field at a certain spatial wavelength that contributes to microturbulent broadening of a line. Stochastic motions on a short scale of heights will fully contribute to the microturbulent broadening of lines; hence for motions with geometrical wavelength $L \ll \lambda$, where λ is the mean free path of the photons, we have $F_\mu = 1$. For motions with $L \gg \lambda$, one has $F_\mu = 0$, while F_μ takes intermediate values for wavelengths in between. For the macroturbulent filter function F_M the reverse is true.

The microturbulent filter function F_μ has been calculated by De Jager & Vermue (1979) and was improved by Durrant (1979) (*cf.* also de Jager, 1981, pp. 47-49). It appears suitable to choose a dimensionless ordinate $k\theta$ or θ/L , where θ is the optical scale height, defined by

$$dz = \theta d \log \tau. \quad (20)$$

The microturbulent filter function used by us is given in Fig. 7, in which the abscissa is $\log(\theta/L)$.

The further procedure is as follows. For defining the 'smooth atmospheric model' we introduce the *average temperature function* $\langle T(\tau) \rangle$ and the *average velocity function* $\langle v(\tau) \rangle$ in the shocked atmosphere. These 'smooth models' were obtained by taking the running averages of $T(\tau)$ and $v(\tau)$ over a distance corresponding to one scale height. We thereupon introduce the function $\Phi(\tau)$, which describes the squared velocities due to the v - and T -fluctuations (which contribute to ζ_μ^2), with

$$\Phi(\tau) = (v(\tau) - \langle v(\tau) \rangle)^2 + \frac{8\Re(T(\tau) - \langle T(\tau) \rangle)}{\pi \times \mu}. \quad (21)$$

Define next a function $Trb(z)$ that describes which part of the atmosphere contributes to the observable microturbulent line broadening:

$$Trb(z) = \Phi(\tau(z)) \times C_L(\tau(z)). \quad (22)$$

Next the *filterfunction* must be introduced. Let $F(1/\alpha)$ be the filter function, where α is a dimensionless unit of length, expressed in units of the average scale height H_{av} . We introduce a function \mathcal{F} being the real part of the Fourier transform of the field of hydrodynamic/thermal velocity fluctuations, and we define the function $\Psi_c(\alpha)$ as

$$\Psi_c(\alpha) = \frac{\int_0^\infty (\mathcal{F}(z/\alpha) \times Trb(z) \times F(1/\alpha)) d\tau(z)}{\int_0^\infty \mathcal{F}(z/\alpha) \times F(1/\alpha) d\tau(z)}. \quad (23)$$

The expected microturbulent velocity component is then found from

$$\zeta_\mu^2 = \int_0^\infty \Psi_c(\alpha)^2 d\alpha. \quad (24)$$

We stress that with the expressions above one finds the value of the *quasi-microturbulence* as we may call it: it is the combined contribution to line broadening by the short-scale variations of the temperature and by those due to short-scale mass motions. If one wishes to know the real hydrodynamic component of it (*i.e.* the effect of mass motions only), the same expressions should be used with the exception that the last (the thermal) part of the *r.h.s.* of Eq. (21) should be dropped. We have done so (see next section), and while finding a *quasi-turbulence* of the order 12 km s $^{-1}$, we find a *hydrodynamic* turbulence of only 0.5 km s $^{-1}$.

9. Application to the case of ρ Cas

We apply the above described algorithms to the hypergiant ρ Cas. There are five input data: T_{eff} , g_{eff} , the maximum Mach number in front of the shocks $M_{1,\text{max}}$, the rate of mass loss \dot{M} , and the luminosity L/L_\odot . These will define output values of T_{eff} , g_{eff} , ζ_μ , v_{hydr} and \dot{M} .

We will show that only T_{eff} and $M_{1,\text{max}}$ really matter. For the luminosity we exclusively used the observed value (*cf.* Table 1), but we know there is an observational tolerance in this parameter, while, if other things remain equal, $L(\cdot)R^2(\cdot)\dot{M}^2$. This proportionality is so obvious that it did not appear necessary to play around with L , but in drawing conclusions the L -dependence should be kept in mind.

In trial calculations we also found rapidly that the input value of \dot{M} does not influence the results as long as the input value remains below $\log \dot{M} < -2.5$. This can be understood because the way \dot{M} enters in the calculations is that it determines the gradient of v_{wind} . Such a gradient could introduce a contribution to the resulting value of ζ_μ , but we found this not to be the case for ρ Cas. For this star this result stands at variance with claims that the observed high microturbulent velocities would be due to the gradient in the stellar wind velocity; *cf.* Lamers & Achmad (1994). We think that their claim is due to the fact that in their study use was made of fictitious lines that originate in the stellar wind, where the relatively strong wind gradient may indeed simulate turbulent line broadening. The observed microturbulent velocities, used in our study (data that were also referred to by Lamers & Achmad), are all derived from spectral lines that are formed in the photosphere in the range of levels approximately defined by the contribution function, shown in Fig. 6. At that level the density is sufficiently high to have $v_{\text{wind}} \approx 0$.

We also found that there is no large variation possible in the input value of g_{eff} ; its value should be chosen only little (*i.e.* ≈ 0.1) below the required (observational) value, which means that the shock wave field only slightly contributes to the effective acceleration.

The input value of T_{eff} should be chosen some 100 to 300 K below the desired (observational) value. This is so, because the many hotter regions behind the shocks enhance the calculated

Table 2. Course of iteration; $\log(L/L_{\odot})=5.7$ and $\log\dot{M}=-6$

$T_{\text{eff},\text{in}}$ (K)	$g_{\text{eff},\text{in}}$	$M_{1,\text{max}}$	$T_{\text{eff},\text{out}}$ (K)	$g_{\text{eff},\text{out}}$	ζ_{μ} (km s $^{-1}$)	v_{hydr} (km s $^{-1}$)	$\log\dot{M}$ (M $_{\odot}$ y $^{-1}$)
6800	2.65	1.07	6930	2.65	11.7	0.6	-4.49
6825	2.70	1.07	7110	2.82	11.7	0.5	-4.70
6830	2.68	1.06	6890	2.80	11.9	0.5	-4.72
6920	2.68	1.06	7150	2.86	11.7	0.4	-4.89

flux and thus we may end up with a shocked photosphere with a somewhat higher effective temperature than the input value.

The only parameter that is really 'free' is the remaining one: $M_{1,\text{max}}$.

To show the course of the iterations we present in Table 2 the results of some trial calculations. The table gives the three input values: T_{eff} , g_{eff} and $M_{1,\text{max}}$. We took in all calculations $\log(L/L_{\odot})=5.7$ (as in Table 1) and $\log\dot{M}=-6$, an arbitrary but unimportant choice.

The gratifying result is that it appears indeed possible to reproduce the observed values for the rate of mass loss as well as that of the high supersonic microturbulent velocity component, the latter being a value that has always surprised observers. These results are obtained by assuming a spectrum of weak shock waves, defined by a largest Mach number $M_{1,\text{max}}=1.06$ to 1.07. The real hydrodynamical component of the motion field (= the fluctuations in v) is small, of the order of 0.4 to 0.6 km s $^{-1}$ only. This result is compatible with current expectations: in Kurucz's models for stars like ρ Cas one would expect a maximum convective velocity of $\simeq 1$ km s $^{-1}$ (cf. Kurucz 1996). The hydrodynamical turbulence is expected to originate in the lower situated convection layer. The observed 'microturbulence' of 11 km s $^{-1}$ would be fully incompatible with this maximum velocity, but the hydrodynamical component derived in this paper, agrees with it.

Another aspect is that repeated calculations for one unique set of input values yield different output data. This is because of the introduction of random phases ϕ in the spectrum of turbulence (Eq. (9)). Physically, this is correct, because also in a stellar atmosphere this would be the case: there is randomness in any spectrum of turbulent motions. For this reason it is not sufficient to end the calculation with one seemingly agreeing set of input parameters. There is a natural spreading in the output data, which should be determined by a number of calculations with the same set of input parameters. An example is shown in Table 3, where such a set is reproduced. From a larger number of such calculations it was found that the scatter in ζ_{μ} and in $\log\dot{M}$ is 0.1 km s $^{-1}$ and 0.07, respectively.

10. Calculated H α line profile from a shocked atmosphere

Spectral observations of ρ Cas occasionally show emission components of the subordinate line H α and of strong resonance lines like those of Ca II. These emission peaks often show a blueward displacement by some 10 km s $^{-1}$. In addition, the central part

Table 3. Integrations for a unique set of input data

$T_{\text{eff},\text{in}}$ (K)	$g_{\text{eff},\text{in}}$	$M_{1,\text{max}}$	$T_{\text{eff},\text{out}}$ (K)	$g_{\text{eff},\text{out}}$	ζ_{μ} (km s $^{-1}$)	v_{hydr} (km s $^{-1}$)	$\log\dot{M}$ (M $_{\odot}$ y $^{-1}$)
6910	2.63	1.06	7420	2.72	11.9	0.5	-4.80
ditto	ditto	ditto	7160	2.67	11.9	0.5	-4.69
ditto	ditto	ditto	7270	2.70	12.0	0.5	-4.91

of the line profile can at times be partly or wholly filled-in by emission.

We think that these aspects can be reconciled by the properties of a shocked atmosphere. The existence of many hot sheets behind the shocks may imply the appearance of emission components in the spectrum. To investigate this aspect, we have calculated a H α line profile for two shocked atmospheres characterized by $T_{\text{eff}}=6991$ K and $g_{\text{eff}}=2.85$, and by $T_{\text{eff}}=7197$ K and $g_{\text{eff}}=2.9$.

Input data for the calculations are the shocked models with the fluctuations of the temperature, electron density, mass density and velocity, all as functions of $\log m$, where m is the mass above the layer of reference.

To perform the non-LTE calculations use was made of coupled equations of radiative transfer and of statistical equilibrium, according to a method that has been described earlier by Scharmer & Carlsson (1985). We used a computer code described by Carlsson (1986). The atmospheric model was approximated by a - slightly smoothed - model. Smoothing was done in order to make the calculations not too cumbersome and primarily to overcome convergence problems.

The theoretical results are given in Fig. 8, and compared with three observed profiles. The comparison shows that the greatly variable aspect of the observed line profile is qualitatively reproduced by the calculations. The significant difference between the two calculated line profiles is in part due to the different input values of T_{eff} , but for another part it reflects the stochastically variable character of the shock-wave field. This is in our feeling an interesting new aspect, worthwhile a study in more depth. We think to have shown by these trial calculations that an atmosphere permeated by shocks, even by weak ones, can yield drastic changes in the emergent H α profile, particularly when also the stellar temperature is changing. The shocked atmosphere apparently succeeds in explaining the strong variations in the profile. However, the asymmetry of the observed H α profile is not reproduced by the calculations.

For the time being we tentatively *conclude* that the general appearance and the strong variability of the H α line profile could be caused by a system of weak shocks in the atmosphere.

11. Conclusions

Among the various remarkable aspects of the hypergiant ρ Cas there are three that we try to explain in this paper: its supersonic microturbulent velocity component, its fairly large rate of mass loss, and the variable appearance of the profile of H α . We based our analysis on the feature that a system of hydrodynamic mo-

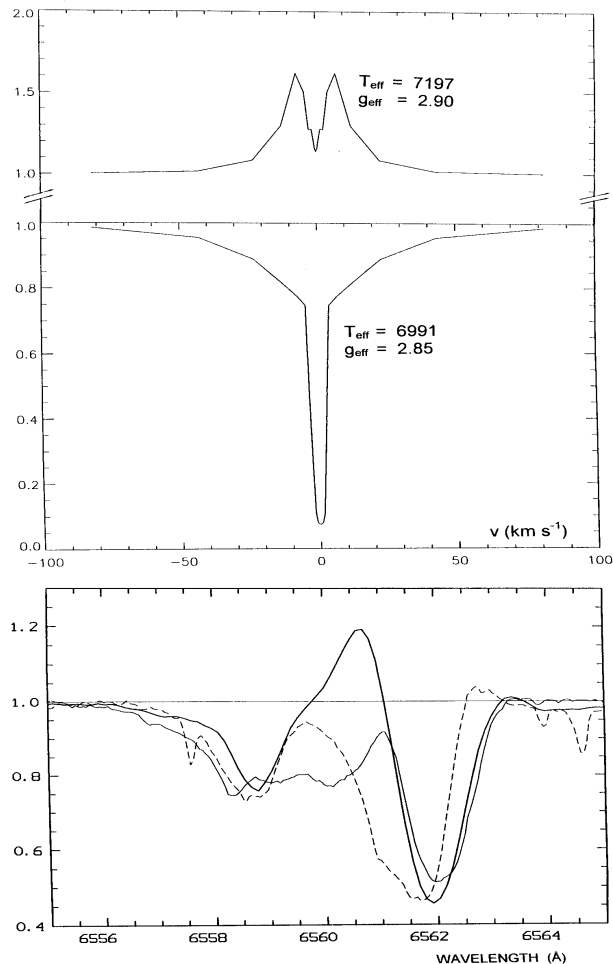


Fig. 8. Calculated and observed line profiles of H α . The calculated profile (upper panel; abscissa is velocity in km s $^{-1}$) is for two input models, defined by: $T_{\text{eff}}=6991$ K and $g_{\text{eff}}=2.85$; $T_{\text{eff}}=7197$ K and $g_{\text{eff}}=2.9$; while also the variations in the outward velocity component have been taken into account. The observations (lower panel; abscissa: Å) are (thick solid line): Nov. 30 '91, courtesy O.R. Stahl; (thin solid line): La Palma Observatory, Dec. 21 '93 and (dashed line): La Palma Observatory, July 25 '94.

tions in the atmosphere of a star with a sufficiently extended atmosphere, such as ρ Cas, is likely to develop into a system of shock waves. We have assumed that these shock waves follow a Kolmogoroff spectrum of turbulence, defined by the maximum Mach number $M_{1,\text{max}}$ in front of the shocks and we have examined the consequences of this assumption. These shocks produce a net mass outflow component, hence they initiate mass loss. The rate of mass loss can be calculated when the velocity- and density-distributions in the shocked atmosphere are known. Furthermore, it appears that in a shocked atmosphere there is not only a quasi-stochastic distribution of velocities, but also of the temperature, the latter being due to the high-temperature sheets behind shocks. Both have their influence on the resulting microturbulent velocity component, but the latter much more than the former.

Calculations show that a maximum shock strength $M_{1,\text{max}}=1.06$ to 1.08 appears to be fully capable of describing the observed rate of mass loss ($10^{-5} M_{\odot} \text{y}^{-1}$) and the supersonic value for the microturbulent velocity component (11 km s^{-1}), while we find at the same time that the purely hydrodynamic component of shock-wave microturbulence is only $\sim 0.5 \text{ km s}^{-1}$, which is a much more reasonable value than the extreme values found when taking the spectral data at their face values. Microturbulence has often been called a 'fudge factor' but such a qualification does not advance the physical understanding. We here claim that the observed 'microturbulent' line broadening is not caused by stochastic small-scale turbulent motions (the classical notion of microturbulence) but by the thermal motions in stochastically distributed high-temperature sheets behind the many shocks.

Another result of this study is that the accumulation of high-temperature sheets behind the many atmospheric shocks produces many relatively hot sheets, particularly in the outer layers of the star (in deeper layers shocks do not so much lead to the appearance of hot sheets because the shock heating is used for ionizing the atmosphere behind the shocks, with small or zero temperature enhancements). A non-LTE calculation of the expected profile of H α shows that a shocked atmosphere is indeed able to simulate the strongly variable displaced emission components.

Finally, we have to refer to the approximations included in the analysis. Most of them have been mentioned in passing. We list them again:

We calculated the values of T_{eff} assuming a gray atmosphere (κ independent of wavelength); we have however tried to compensate that approximation by a strictly differential approach.

The accumulation of the wakes of shocks and its influence on the temperature structure of the atmosphere was handled in a first-order way. More refined methods can be thought of.

The calculation of the 'standard' v - and $\log \rho$ -profiles in the shocks, as described in Sect. 3, was done assuming an isothermal situation, while we know that the gas behind the shocks is not isothermal. There exist refined, but cumbersome methods for calculating the velocity and density profiles behind shocks, but for reducing computer time we did not want to use them in the present study.

We did not include the effect of pulsations, while recent observations suggest a certain degree of correlation between strong pulsations and periods of enhanced mass loss.

Acknowledgements. A.L. acknowledges financial support by the Fund for Scientific Research - Flanders (Belgium) in 1995-97. G.I. wishes to express his sincere thanks to Prof. J.P. de Greve in Brussels for his hospitality and to Dr. M. Carlsson for stimulating discussions. We thank O.R. Stahl for putting spectral observations at our disposal. Hans Nieuwenhuijzen's invaluable help in many computer problems is mentioned with thanks. We are obliged to Prof. Michael Grewing for a number of very useful comments on a first draft. The suggestions from an unknown referee are thankfully acknowledged.

References

- Achmad L., de Jager C., Nieuwenhuijzen H., 1991, A&A 250, 445
- Arellano Ferro A., 1985, MNRAS 216, 571
- Beardsley W.R., 1961, ApJS 5, 381
- Carlsson M., 1986, Ups. Astron. Obs. Rep., no. 33
- Climenhaga J.L., Gesicki K., Smolinski J., 1992, in C. de Jager and H. Nieuwenhuijzen (eds), *Instabilities in evolved super- and hypergiants*, North Holland, Amsterdam, p. 82
- de Jager C., 1981, *The Brightest Stars*, Reidel, Dordrecht
- de Jager C., Vermue J., 1979, Ap. Space Sci., 61, 129
- de Jager C., Nieuwenhuijzen H., van der Hucht K.A., 1988, A&AS 72, 259
- de Jager C., De Koter A., Carpay J., Nieuwenhuijzen H., 1991, A&A 244, 131
- Dere K.P., 1989, ApJ 340, 599
- Durrant C.J., 1979, A&A 73, 137
- Gail H.P., Cuntz M., Ulmschneider P., 1990, A&A 234, 359
- Gesicki K., 1992, A&A 254, 280
- Kurucz R., 1996, in S.J. Adelman, F. Kupka, W.W. Weiss, (eds.): *Model Atmospheres and Spectrum Synthesis*, ASP Conf. Ser. 108
- Lambert D.L., Hinkle K.H., Hall D.N.B., 1981, ApJ 248, 638
- Lamers H.J.G.L.M., Achmad L., 1994, A&A 291, 856
- Lobel A., de Jager C., 1997, A&A, submitted
- Lobel A., Achmad L., de Jager C., Nieuwenhuijzen H., 1992, A&A 256, 159
- Lobel A., de Jager C., Nieuwenhuijzen H., Smolinski J., Gesicki K., 1994, A&A 291, 226
- Lobel A., Israelian G., de Jager C., Musaev F., Parker J. Wm., Mavrogiorgou A., 1997 A&A, submitted
- Nieuwenhuijzen H., De Jager C., Cuntz M., 1994, A&A 285, 595
- Nieuwenhuijzen H., de Jager C., Cuntz M., Lobel A., Achmad L., 1993, A&A 280, 195
- Percy J.R., Fabro V.A., Keith D.W., 1985, JAAVSO, 14, 1
- Sargent W.L.W., 1961, ApJ 134, 142
- Scharmer G.B., Carlsson M., 1985, J. Comput. Phys. 59, 56
- Sheffer Y., Lambert D.L., 1986, PASP 98, 914 and 99, 1272
- Spiegel E.A., 1957, ApJ 126, 202
- Zsoldos E., Percy J.R., 1991, A&A 264, 441